Fluid interactions that enable stealth predation by the upstream foraging hydromedusa *Craspedacusta sowerbyi*

Lucas K[1], Colin SP[1,2,*], Costello JH[2,3], Katija K[4], Klos E[5]

1. Biology, Roger Williams University, Bristol, RI 02809
2. Whitman Center, Marine Biological Laboratories, Woods Hole, MA 02543
3. Biology Department, Providence College, Providence, RI 02918
4. Applied Ocean Physics and Engineering, Woods Hole Oceanographic Institute, Woods Hole, MA 02543
5. Graduate School of Oceanography, University of Rhode Island, Narragansett, RI 02882

Running head: Stealth predation by hydromedusae
Key Words: Hydromedusae, foraging, stealth predation, encounter rate, jellyfish

*To whom correspondence should be addressed. Email: scolin@rwu.edu

Abstract

Unlike most medusae which forage with tentacles trailing behind their bells, several species forage upstream of their bells using aborally located tentacles. It has been hypothesized that these medusae forage as stealth predators by placing their tentacles in more quiescent regions of flow around their bells. Consequently, they are able to capture highly mobile, sensitive prey. In this study, we used digital particle image velocimetry (DPIV) to quantitatively characterize the flow field around *Craspedacusta sowerbyi*, a freshwater upstream foraging hydromedusa, to evaluate the mechanics of its stealth predation. We found that fluid velocities were minimal in front and along the sides of the bell where the tentacles are located. As a result, the deformation rates in the regions where the tentacles are located were low, below the threshold rates required to elicit an escape response in several species of copepods. Estimates of their encounter volume rates were examined based on flow past the tentacles and trade-offs associated with tentacle characteristics were evaluated.

INTRODUCTION

Hydromedusae exhibit a broad morphological and functional diversity that enable them to occupy a variety of trophic roles (Mills 1981, Colin & Costello 2002, Colin et al. 2003, Colin et al. 2006). Often acting as dominant predators in coastal ecosystems, hydromedusae substantially affect zooplankton prey populations (Larson 1987, Purcell & Grover 1990, Matsakis & Conover 1991, Purcell 2003, Jankowski et al. 2005). Understanding the factors underlying foraging can provide insight into trophic impact of hydromedusae. Because propulsive mode, swimming performance, bell morphology, and prey selection are all thought to be directly linked to foraging behavior, analysis of these features ultimately fosters an understanding of ecological role.

Feeding rates and predatory impact of zooplanktivores are determined by the rate at which they encounter and retain prey. For most pelagic predators, predation is a function of encounter volume rate, defined as the volume of water the predator can search per unit time (Gerritsen & Strickler 1977, Kiørboe 2008, Colin et al. 2010, Kiørboe 2011). The manner in which medusa interact with their surrounding fluid affects their encounter volume rate and, therefore, their predation, because medusa feeding and swimming are interrelated processes (Mills 1981, Daniel 1983, 1985, Costello 1992, Costello & Colin 1994, Sullivan et al. 1994, Costello & Colin 1995, Ford et al. 1997, D'ambra et al. 2001). As such, propulsive modes can be used to broadly describe feeding types, and wake structures have been used to categorize medusan species into two propulsive modes: jetting and rowing (Colin & Costello 2002).

Jetting medusae are characterized by having small, prolate bells (fineness ratio >0.5) and constricted orifices leading to the subumbrellar cavity (Daniel 1983, 1985, Colin & Costello

2002, Dabiri et al. 2006). Swimming is characterized by rapid, full-body contractions of the bell that propel jets of fluid from the subumbrellar cavity (Daniel 1983, 1985, Colin & Costello 2002, Dabiri et al. 2006). This mechanism maximizes thrust (Daniel 1985, Dabiri et al. 2006), but these medusae are constrained by size, since force required for jet propulsion increases more rapidly than available physiological force as bell diameter increases (Dabiri et al. 2007, Costello et al. 2008). The jet production has a high energy cost (Daniel 1983, 1985, Dabiri et al. 2006), so jetting medusae drift the majority of the time, foraging as ambush predators (Colin et al. 2003, Hansson & Kiørboe 2006).

In contrast, rowing medusae have oblate bells (fineness ratio <0.5) and are not constrained by size (Dabiri et al. 2007). In these medusae, the bell margin acts as a paddle during bell pulsations, producing starting and stopping vortices rotating in opposite directions relative to one another that are shed from alongside the bell (Dabiri et al. 2005). Thrust is generated by the interaction of these vortices, providing a slower but more energy-efficient mode of swimming (Dabiri et al. 2005, Dabiri et al. 2007, Sahin et al. 2009, Dabiri et al. 2010). Additionally, this process produces a long, trailing vortex ring wake structure, which entrains large volumes of water behind the bell during both contraction and expansion phases of the pulse cycle (Dabiri et al. 2005). This is advantageous in drawing prey onto capture surfaces located in this region of maximum flow throughout the entire duration of the pulse (Larson 1991, Dabiri et al. 2005). With these minimal energy costs and high circulation through trailing capture surfaces, rowing medusae forage continuously as feeding-current feeders (Colin & Costello 2002, Colin et al. 2003, Kiørboe 2011).

To feed, predators must accompany an encounter with a successful capture, in which they strike and retain prey before the prey can detect and evade the predator. Tentacles are used by

47 medusae for prey capture, and accordingly, tentacle morphology (number, thickness, and
48 posture) has been shown to contribute to foraging behavior and prey selection (Mills 1981,
49 Madin 1988, Costello & Colin 1995, Raskoff 2002, Colin et al. 2006). For example, several
50 lineages of rowing medusae forage with their tentacles positioned aborally, in front of the bell
51 (termed upstream foragers). While their tentacle placement differs from typical rowing species
52 with orally-positioned trailing tentacles, these upstream foragers maintain the same surrounding
53 flow structure as typical rowing medusae (Colin et al. 2006). This upstream tentacle posture
54 removes capture surfaces from the region where the trailing vortex rings circulate, and flow is
55 characterized by high flow velocities and shear deformation rates (Colin et al. 2006). This is
56 important because many zooplankton detect fluid disturbances generated by an approaching
57 predator, such as this high circulation region behind a rowing medusa, and respond with an
58 escape reaction (Kiørboe et al. 1999, Kiørboe & Visser 1999, Suchman 2000). Fluid upstream of
59 a rowing medusa's bell, however, is less disturbed (Raskoff 2002, Colin et al. 2006, Sørnes et al.
60 2008). It has been suggested that positioning tentacles aborally enables upstream foragers to act
61 as stealth predators (Raskoff 2002, Colin et al. 2006, Sørnes et al. 2008). Although considerable
62 data exists documenting the hydrodynamics and prey selection of downstream-foraging medusae
63 (Costello & Colin 1994, Sullivan et al. 1994, Costello & Colin 1995, Ford et al. 1997, D'ambra et
64 al. 2001, Colin & Costello 2002, Colin et al. 2003), the fluid interactions of upstream foragers
65 have not been examined quantitatively.
66 This study addresses this issue by examining the fluid interactions in *Craspedacusta*
67 *sowerbyi*, a freshwater, upstream-foraging, rowing hydromedusa (Hydrozoa: Olindiidae).
68 Originating in the Yangtze river system in China, *C. sowerbyi* has been introduced in small
69 lakes, ponds, and water-filled quarries in North America, Europe, and Asia (Kramp 1951), where

it is known to prey on motile, sensitive zooplankton such as rotifers, copepods, and cladocerans in the 0.2-2 mm size range (Dodson & Cooper 1983, Spadinger & Maier 1999, Jankowski et al. 2005). Here, we quantify morphological characteristics, fluid flows around swimming individuals, and estimates of encounter volume rate to evaluate the mechanics of *C. sowerbyi*'s stealth predation.

METHODS

Video recording. Individual hydromedusae were hand collected in jars by scuba divers and were immediately transported to lab for analysis. Digital photographs and video recordings (SVHS) were made for tentacle counts using white lighting following the methods of Costello and Colin (1994) and Colin and Costello (2002). Spatial characteristics of the optical field were determined from scale bars periodically included in the original recordings. Morphological measurements such as bell diameter and tentacle length were made directly from recordings calibrated with scale bars.

Quantitative flow measurements were made in the laboratory using 2D DPIV following the methods of Colin et al. (2010). Individual medusae were illuminated through the center of the animal body with a laser sheet (680-nm wavelength). Laser light sheet alignment was identified when the manubrium was fully illuminated, and only sequences where the medusa swam perpendicular to the screen were selected for analysis to ensure that there was no motion in the unmeasured third dimension. Video was recorded at 500 frames s^{-1} using a high-speed digital video camera (Fastcam 1024 PCI; Photron) placed perpendicular to the light sheet. Illuminated particle velocity was determined from sequential images analyzed by a cross-correlation algorithm (LaVision Software). This analysis generated velocity vector fields around the medusa.

93 For further analysis, the each individual's fluid interactions were characterized at six
94 instances throughout the pulsation cycle, where the first instance in the series had a fully-relaxed
95 bell and the fourth had a fully-contracted bell. The second and third instances corresponded to
96 two times equally spaced between the relaxed and contracted states, and similarly, the fifth and
97 sixth instances corresponded to two times equally spaced between the contracted state and
98 relaxed state marking the beginning of the next pulse cycle.
99 **Morphological analysis.** Total tentacle count was estimated based on tentacle counts reported in
100 the literature (Mayer 1910, Payne 1924, Boulenger & Flower 1928, Fantham & Porter 1938,
101 Kramp 1951, Russell 1953, Pennak 1956). Tentacles were further divided into three distinct size
102 classes: long, medium, and short. Several still images from the VHS recordings in which the
103 medusa's aboral surface was oriented toward the camera were selected for a count of tentacles in
104 the medium size category. The mean of these counts provided an estimate of the number of
105 medium-length tentacles. The long-length tentacle category contained only the 4 perradial
106 tentacles (Kramp 1951). The number of small-length tentacles fringing the bell was the
107 difference between the total count and sum of the number of medium and long tentacles.
108 Using the PIV video sequences, tentacles on one side of the medusa were digitized as
109 series of points using ImageJ (developed by the NIH) software. Tentacle length was measured
110 by summing the distances between successive points. Angle from vertical (θ) was also measured
111 using this software.
112 Gap width between tentacles (Figure 2) was calculated as a fraction of the circumference
113 of a circle obtained by looking down on the bell. This circle had a radius R, given by

$$R = r_{bell} + L_x(x_i)$$

114 Equation 1

where r_{bell} was the bell radius and $L_x(x_i)$ was the length along a tentacle's projection onto the *x*-plane at position *i* along the tentacle, such that

$$L_x(x_i) = L_{T,i} \sin \theta_m$$

Equation 2

where $L_{T,i}$ was the distance from the bell to position *i* measured along the tentacle and θ_m was the angle of the medium tentacles from vertical. To account for tentacle thickness, the diameter of a medium-length tentacle (D_{Tm}) was subtracted. Thus, the gap width (W) was calculated as

$$W = \frac{1}{N}(\pi D) - D_{Tm}$$

Equation 3

where *N* was the number of tentacles of length $L > L_{T,i}$.

Maximum area of tentacle sweep (*S*) was found using the surface of revolution formula for a function *f(x)* (Larson et al. 2007),

$$S = 2\pi \int_{x_{i-1}}^{x_i} r(x)\sqrt{1 + (f'(x))^2}dx$$

Equation 4

The tentacle was approximated as a series of lines connecting the successive points with *x*-coordinates x_i and x_{i+1}, so

$$f'(x) = m$$

Equation 5

where *m* was the slope of the line, and since the axis of rotation was the vertical axis through the bell's apex, a position defined as $x = 0$, *r(x)*, the distance between *f(x)* and the axis of rotation, was

$$r(x) = x$$

Equation 6

Substituting and solving the integral led to the formula describing the maximum area swept by the tentacle array:

$$S = \sum_{i=2}^{n} \pi\sqrt{1+m^2}({x_i}^2 - {x_{i-1}}^2)$$

Equation 7

Kinematic Analysis. Frames were extracted from the PIV video sequences at 0.02-s time intervals (t), and medusa motion was measured from sequential changes in position (x, y) of the anterior-most point of the exumbrellar surface. Bell velocity (U_{bell}) for each time interval was calculated as:

$$U_{bell} = \frac{\sqrt{(x_{n+1} - x_n)^2 + (y_{n+1} + y_n)^2}}{t}$$

Equation 8

The relative velocity (u_i) between water moving across the tentacle and the medusa at point i along the length of the tentacle was calculated as:

$$u_i = u_{w,y,i} - U_{bell} sin\theta$$

Equation 9

where $u_{w,y,i}$ was the component of water velocity (obtained from the PIV output) in a direction perpendicular to the tentacle at point i. Because the medusae were positioned such that the tentacles were not directly aligned with the laser sheet, this calculation resulted in free-stream

relative fluid velocities between adjacent tentacles rather than velocities in the tentacle boundary layer.

Localized Reynolds number ($Re_{Dt,i}$) at position *i* along the length of the tentacles was approximated using the formula

$$Re_{Dt,i} = \frac{D_T|u_i|}{\nu}$$

Equation 10

where ν was the kinematic viscosity of freshwater, and D_T was the tentacle diameter (D_{Tm} was used until position *i* along tentacle exceeded the length of a medium tentacle, after which D_{Tl}, the diameter of a long tentacle, was used) (Denny 1993, Vogel 1994, Colin & Costello 2002).

$Re_{Dt,i}$ was then used to estimate boundary layer thickness (δ_i) along the length of the tentacles using the formula:

$$\delta_i = 0.8\frac{D_T}{\sqrt{Re_{Dt,i}}}$$

Equation 11

where, as before, D_{Tm} was used until position *i* along tentacle exceeded the length of a medium tentacle, after which D_{Tl} was used (Feitl et al. 2009).

The velocity vector fields generated in the DPIV analysis enabled measurement of the four components of 2D shear deformation rates (rate of strain) E_{xx}, E_{xy}, E_{yx}, E_{yy} in the flow field, calculated with the equation set below

$$E_{xx} = \frac{du_x}{dx}$$

$$E_{xy} = \frac{du_y}{dx}$$

$$E_{yx} = \frac{du_x}{dy}$$

$$E_{yy} = \frac{du_y}{dy}$$

Equation 12

where *u* was the measured planar velocity field. The maximum of these components was used to represent the maximum deformation rate (Colin et al. 2010), since a copepod prey item will elicit an escape response when the deformation rate is greater than its threshold regardless of its direction (Kiørboe et al. 1999, Kiørboe & Visser 1999).

RESULTS

Flow field around swimming medusae

Bell pulsations generated a flow field characteristic of rowing medusae, with fluid accelerating orally and becoming entrained in a trailing vortex ring wake structure (Figure 3). The velocity of fluid surrounding the medusa varied spatially around the bell. Upstream of the medusa, the velocity of the fluid was low relative to the flow downstream throughout the swimming cycle. In the region directly alongside the aboral face, upstream fluid velocities increased during states nearing maximum contraction when the medusae's swimming velocity peaked, approaching 10 mm/s, but remained lower than fluid velocities downstream of the medusa, where velocity was in the excess of 25 mm/s in the vortex ring wake structure (Figure 3). Throughout the entire duration of the pulsation cycle, the lowest fluid velocities were observed in the region alongside the bell containing the tentacles, and additionally, this region showed minimal velocity gradients (Figure 3). Peak fluid velocity occurred in the downstream wake region during maximum contraction (t = 0.16; Figure 3).

In a similar manner, the magnitude of the maximum directional component of the shear deformation rate (rate of strain) varied spatially around the bell. Upstream of the bell, the maximum directional component was low, exceeding ~3-4 s^{-1} only in regions directly alongside the aboral face of the bell during times approaching maximum contraction (Figure 4, 5). This corresponded to the observed increases in fluid velocities (Figure 3). The lowest deformation rates occurred alongside the bell, in the region containing the tentacles. With few exceptions (where deformation rate approached 5 s^{-1} near the distal end of the tentacle), the deformation rates along the tentacles were <3 s^{-1} (Figure 4, 5). In contrast, maximum deformation rates, >10 s^{-1} and peaking near 30 s^{-1}, occurred downstream of the bell, in the vortex ring wake structure (Figure 4, 5).

Tentacle kinematics

The profiles of the fluid velocity relative to the tentacles maintained a characteristic shape throughout the duration of the pulse cycle but varied in the velocity magnitudes associated with each profile. The relative velocity (u_i) of fluid crossing the proximal end of the tentacle approached 0 mm/s (Figure 6). This demonstrated that fluid in the bell's boundary layer translated negligibly relative to the tentacle. Velocities across the tentacles increased away from the bell and remained constantly high beyond the length of the short set of tentacles. In fact, fluid moved across the tentacles throughout the pulse but peaked when the medusae's swimming velocity peaked. The existence of this flow field allowed for boundary layer development on the tentacles.

The boundary layer of the bell could be seen in the low relative velocities near the bell and extended to the tips of the short tentacles. As a result of the low flow over the short tentacles

and the close proximity of adjacent tentacles, flow was greatly constricted between the short tentacles. To examine if flow passes between the short tentacles, we compared the boundary layer thickness around the short tentacles to the gap width between tentacles. The smallest gaps between tentacles occurred directly alongside the bell, within the length of the short-length class tentacles (Figure 7). Within this region, the thickness of the boundary layer around the tentacles was often greater than the gap width between tentacles, except during parts of the pulse where flow peaked (Figure 7 states 2-4). During peak flow, the boundary layer (defined as the region from the no slip condition to 99% free stream flow) was about the same size as the gaps, so during these times flow would be constricted but some fluid would pass between the smallest tentacles. During other times in the pulse, the boundary layer thickness was greater than the gap width and little to no fluid passed between the tentacles (Figure 7).

Beyond the length of the short-class tentacles, gap width between tentacles far exceeded the thickness of boundary layers on tentacles (Figure 7), indicating that encountered fluid could pass freely between tentacles in this region. These results were consistent with the relative velocity profiles on the tentacles, which showed that fluid motion relative to the bell was minimal along the length of the short tentacles (Figure 7), as well as with observations of particle motions in the PIV video sequences.

DISCUSSION

Flow and prey detection

To successfully capture fast, motile zooplankton prey, stealth predators approach their prey with minimal fluid disturbances. Unlike medusae with trailing tentacles whose capture surfaces are located in highly disturbed flow, the tentacles of *Craspedacusta sowerbyi* are positioned upstream of the bell in a region characterized by low fluid velocities. Therefore, it has

been suggested that *C. sowerbyi* and other medusae with tentacles positioned upstream forage as stealth predators. Quantitative analysis of the flow around swimming *C. sowerbyi* confirms that the aborally positioned tentacles are in regions where deformation rates of the fluid are below the documented response thresholds of copepods (Figure 4, 5; Table 1). As a result, it is expected that *C. sowerbyi,* and other upstream foragers, are capable of approaching copepods and other sensitive zooplankton without detection, which confirms previous speculation (Raskoff 2002, Colin et al. 2006, Sørnes et al. 2008).

The idea that *Craspedacusta sowerbyi* uses stealth predation to capture prey is also supported by prior laboratory incubation studies where *C. sowerbyi* has been shown to readily consume copepods along with less reactive, slower prey such as rotifers and cladocerans (Dodson & Cooper 1983, Spadinger & Maier 1999, Jankowski et al. 2005). However, prey size versus clearance rate data presented by Dodson and Cooper (1983) demonstrates a trade-off faced by medusae which forage as upstream predators. Their data showed that clearance rates on slow, less reactive prey, such as rotifers and cladocerans, increased with prey size while clearance rates on fast, reactive copepods decreased with prey size (Dodson & Cooper 1983). This suggests that encounter rates limit ingestion of less reactive prey while capture efficiencies limit ingestion on highly reactive prey.

For upstream foraging medusae, the tentacle array will primarily determine encounter rates (Madin 1988) and capture efficiencies (Colin et al. 2006). The number of upstream tentacles should be directly related to encounter rates with less reactive prey since this will increase capture surfaces and decrease spacing between tentacles. However, as tentacle density increases so would the fluid disturbances upstream of the medusae due to the boundary layer and drag of the tentacles. Copepods, the most sensitive prey type of *Craspedacusta sowerbyi*, detect

shear deformation rates in their surrounding fluid to detect predators. If deformation rates are greater than a detection threshold, copepods will react with an escape response and jump away from the predator (Kiørboe et al. 1999, Kiørboe & Visser 1999). The fluid disturbances generated by the upstream tentacles of *C. sowerbyi* were below the average detection limits of copepods whose thresholds have been measured (Figure 4, 5; Table 1). However, shear deformation rates were above copepod detection limits along the boundary layer of the bell surface and the smallest set of tentacles. High deformation rates in regions with dense tentacle assemblages support the expectation that too many tentacles may reduce the ability of upstream foragers to encounter copepods undetected. Consequently, the observed tentacle arrays of upstream foragers are likely the result of a trade-off between high tentacle densities that maximize prey encounter rates and low tentacle densities that minimize detection by prey.

Flow and prey encounter

Fluid flowing through the tentacles array carries planktonic prey and is the basis for prey capture by *Craspedacusta sowerbyi*. *C. sowerbyi* possesses three distinct groups of tentacles differing in length, thickness, and abundance. Based on our estimates of fluid flows and tentacle dimensions, during periods of peak fluid velocities (states 2 and 3; Figure 6) we expect some fluid to pass between even the smallest, most densely packed tentacles along the bell margin, especially at the tips of these tentacles (Figure 7). Video observations confirm that particles were able to pass between these tentacles during limited portions of the swim cycle. We expect that the small tentacle group likely serves to capture primarily small zooplankton. In contrast, fluid passed freely between the medium and long groups of tentacles. Consequently, we expect these regions to be the primary prey capture regions for most of the larger prey.

Direct observations of prey retention in the field by *Craspedacusta sowerbyi* are not available, but hydromechanical information provides a basis for estimation of the dominant mechanisms determining prey encounter with the tentacles. Upstream foraging medusae use their tentacles to capture prey either by sieving the flow, resulting in capture of prey larger than the inter-tentacle gaps, or by retaining prey which are smaller than the distance between the tentacles via a direct interception. The encounter volume rate (EVR) with prey is determined by the volume of fluid that passes through the tentacles over time. For upstream foraging medusa, this can be approximated from the product of the relative fluid velocity across the tentacles and the conical surface area of the tentacle assemblage (Hansson & Kiørboe 2006, Kiørboe 2011). Accordingly, *C. sowerbyi*'s sieving EVR was estimated as 7.11 ± 2.59 L hr^{-1} (Table 2). This estimate would be appropriate for medusae such as *Solmissus* spp. which forage on gelatinous prey that are frequently larger than the inter-tentacle gaps (Raskoff 2002, Colin et al. 2006). However, it is not representative of species like *Periphylla periphylla* (Sørnes et al. 2008) or *C. sowerbyi* which forage on crustacean prey that are much smaller than the inter-tentacle gaps. A more appropriate approximation of EVR for *C. sowerbyi* assumes that the dominant prey encounter mechanism is direct interception and relies upon Re ranging from 0.2-2 around the tentacles. We can estimate the EVR using intermediate Re estimates (Humphries 2009) so that

$$EVR = 2U_{mean}L_T\lambda N$$

Equation 13

where U_{mean} is the average flow velocity along the tentacle and λ is an empirically derived value from Humphries (2009) that is based on prey size (for *C. sowerbyi* mean prey size is 1.1 mm) and describes the width of flow that will cause prey to intercept a cylinder (i.e.; tentacle). Based

296 on these calculations, the EVR for *C. sowerbyi* is 1.4 ± 0.50 L hr^{-1} (Table 2). This EVR is
297 considerably lower than the EVR estimate for sieving large prey. However, it is considerably
298 larger than reported empirical clearance rates, which were an average of 0.01 L $predator^{-1}$ hr^{-1} (or
299 maximum 0.04; Table 2).

300 The EVR estimates for direct interception of prey by *Craspedacusta sowerbyi* represent
301 an upper potential clearance rate that assumes 100% capture of prey encountered by the
302 medusae. High capture rates of encountered prey can occur with some gelatinous predators, such
303 as the ctenophore *Mnemiopsis leidyi* (Costello et al. 1999). However, capture rates for other
304 upstream foraging medusae feeding on copepods appear to be low. For example, the
305 scyphomedusa *Nausithoë punctata* (Colin et al. 2006) captured relatively few of the crustacean
306 prey it encountered (adult copepods = 2% and nauplii = 12%). Additionally, small zooplankton
307 may not activate the tentacle's nematocysts (Madin 1988, Spadinger & Maier 1999).
308 Consequently, low capture rates can result in clearances rates that are considerably less than
309 encounter volume rates. Additionally, the EVR estimate assumes constant swimming but prior
310 behavioral observations indicate that *C. sowerbyi* spends only ~70% of its time swimming
311 (Colin et al. 2006). Rather than by continuous swimming, *C. sowerbyi* forages by swimming up
312 the water column, flipping over, and passively sinking back down the water column with
313 tentacles extended (Milne 1938, Kramp 1951). If the tentacles are oriented in swimming
314 direction, they may still serve to encounter prey whether the medusae is actively pulsing or
315 passively sinking. This may be a potential adaptive advantage of upstream positioned tentacles.
316 However, the different swimming behaviors entail different flow velocities past the tentacles,
317 and therefore, cause deviations from the assumption of continuous swimming that underlies EVR
318 estimates. One pathway to resolution of the differences between potential and realized clearance

319 rates requires determining the details of encounter events, e.g. Regula et al. (2009), between *C.*
320 *sowerbyi* and its prey. Rates of these biological interactions could provide information to modify
321 physically-based estimates such as EVR to create a more realistic model of the physical-
322 biological interactions that ultimately determine medusan foraging rates.
323
324 *Acknowledgements*. We thank Edmund and Julia for their generous hospitality and guidance
325 during the collecting trip and the reviewers for valuable comments that improved earlier versions
326 of the manuscript. This research is supported by the National Science Foundation awarded to
327 SPC (OCE- 0623534 and 0727544) and JHC (OCE-0351398 and OCE-0623534) and by the
328 Office of Naval Research awarded to JHC (N000140810654). K.Lucas was partially funded by
329 EPSCoR Cooperative Agreement #EPS-1004057 to the State of Rhode Island SURF award. S.
330 Colin was also supported by RWU Foundation to Promote Scholarship and Teaching.
331

LITERATURE CITED

Boulenger CL, Flower WU (1928) *Craspedacusta sowerbii*, and its identity with *c. (microhydra) ryderi.* Proc Zool Soc Lond 98:1005-1014

Burdick DS, Hartline DK, Lenz PH (2007) Escape strategies in co-occurring calanoid copepods. Limnol Oceanogr 52:2373-2385

Colin SP, Costello JH (2002) Morphology, swimming performance and propulsive mode of six co-occurring hydromedusae. J Exp Biol 205:427-437

Colin SP, Costello JH, Hansson LJ, Titelman J, Dabiri JO (2010) Stealth predation and the predatory success of the invasive ctenophore *mnemiopsis leidyi*. Proc Natl Acad Sci USA 107:17223-17227

Colin SP, Costello JH, Klos E (2003) *In situ* swimming and feeding behavior of eight co-occurring hydromedusae. Mar Ecol Prog Ser 253:305-309

Colin SP, Costello JH, Kordula H (2006) Upstream foraging by medusae. Mar Ecol Prog Ser 327:143-155

Costello JH (1992) Foraging mode and energetics of hydrozoan medusae. Scientia Marina 56:185-191

Costello JH, Colin SP (1994) Morphology, fluid motion and predation by the scyphomedusa *aurelia aurita*. Mar Biol 121:327-334

Costello JH, Colin SP (1995) Flow and feeding by swimming scyphomedusae. Mar Biol 124:399-406

Costello JH, Colin SP, Dabiri JO (2008) Medusan morphospace: Phylogenetic constraints, biomechanical solutions, and ecological consequences. Invertebrate Biology 127:265-290

Costello JH, Loftus R, Waggett R (1999) Influence of prey detection on capture success for the ctenophore *mnemiopsis leidyi* feeding upon adult *acartia tonsa* and *oithona colcarva* copepods. Mar Ecol Prog Ser 191:207-216

D'ambra I, Costello JH, Bentivegna F (2001) Flow and prey capture by the scyphomedusa *phyllorhiza punctata* von lendenfeld, 1884. Hydrobiologia 451:223-227

Dabiri JO, Colin SP, Costello JH (2006) Fast-swimming hydromedusae exploit velar kinematics to form an optimal vortex wake. J Exp Biol 209:2025-2033

Dabiri JO, Colin SP, Costello JH (2007) Morphological diversity of medusan lineages constrained by animal-fluid interactions. J Exp Biol 210:1868-1873

Dabiri JO, Colin SP, Costello JH, Gharib M (2005) Flow patterns generated by oblate medusan jellyfish: Field measurements and laboratory analyses. J Exp Biol 208:1257-1265

Dabiri JO, Colin SP, Katija K, Costello JH (2010) A wake-based correlate of swimming performance and foraging behavior in seven co-occurring jellyfish species. J Exp Biol 213:1217-1225

Daniel TL (1983) Mechanics and energetics of medusan jet propulsion. Can J Zool 61:1406-1420

Daniel TL (1985) Cost of locomotion: Unsteady medusan swimming. J Exp Biol 119:149-164

Denny M (1993) Air and water: The biology and physics of life's media, Vol. Princeton University Press, Princeton, NJ

Dodson SI, Cooper SD (1983) Trophic relationships of the freshwater jellyfish *craspedacusta sowerbyi* lankester 1880. Limnol Oceanogr 28:345-351

Fantham HB, Porter A (1938) Occurrence of the freshwater medusa, *craspedacusta sowerbii*, in eastern canada. Nature 141:515-516

Feitl KE, Millet AF, Colin SP, Dabiri JO, Costello JH (2009) Functional morphology and fluid interactions during early development of the scyphomedusa *aurelia aurita*. Biol Bull 217:283-291

Ford MD, Costello JH, Heidelberg KB, Purcell JE (1997) Swimming and feeding by the scyphomedusa *chrysaora quinquecirrha*. Mar Biol 129:355-362

Gerritsen J, Strickler JR (1977) Encounter probabilities and community structure in zooplankton: A mathematical model. J Fish Res Board Can 34:73-82

Green S, Visser A, Titelman J, Kiørboe T (2003) Escape responses of copepod nauplii in the flow field of the blue mussel, *mytilus edulis*. Mar Biol 142:727-733

Hansson LJ, Kiørboe T (2006) Prey-specific encounter rates and handling efficiencies as causes of prey selectivity in ambush-feeding hydromedusae. Limnol Oceanogr 51:1849-1858

Humphries S (2009) Filter feeders and plankton increase particle encounter rates through flow regime control. Proc Natl Acad Sci USA 106:7882-7887

Jankowski T, Strauss T, Ratte HT (2005) Trophic interactions of the freshwater jellyfish *craspedacusta sowerbii*. J Plankton Res 27:811-823

Kiørboe T (2008) A mechanistic approach to plankton ecology, Vol. Princeton University Press, Princeton, NJ

Kiørboe T (2011) How zooplankton feed: Mechanisms, traits and trade-offs. Biol Rev 86:311-339

Kiørboe T, Saiz E, Visser A (1999) Hydrodynamic signal perception in the copepod *acartia tonsa*. Mar Ecol Prog Ser 179:97-111

Kiørboe T, Visser A (1999) Predator and prey perception in copepods due to hydromechanical signals. Mar Ecol Prog Ser 179:81-95

Kramp PL (1951) Freshwater medusae in china. Proc Zool Soc Lond 120:165-184

Larson R, Hostetler R, Edwards BH (2007) Calculus of a single variable, Vol. Houghton Mifflin Company, Boston, MA

Larson RJ (1987) Trophic ecology of planktonic gelatinous predators in saanich inlet, british columbia: Diets and prey selection. J Plankton Res 9:811-820

Larson RJ (1991) Diet, prey selection, and daily ration of *stomolophus meleagris*, a filter-feeding scyphomedusa from the ne gulf of mexico. Estuar Coast Shelf Sci 32:511-525

Madin LP (1988) Feeding behavior of tentaculate predators: *In situ* observations and a conceptual model. Bull Mar Sci 43:413-429

Matsakis S, Conover RJ (1991) Abundance and feeding of medusae and their potential impact as predators on other zooplankton in bedford basin (nova scotia, canada) during spring. Can J Fish Aquat Sci 48:1419-1430

Mayer AG (1910) Medusae of the world vol. 1: The hydromedusae, Vol. Carnegie Institute of Washington, Washington, DC

Mills CE (1981) Diversity of swimming behaviors in hydromedusae as related to feeding and utilization of space. Mar Biol 64:185-189

Milne LJ (1938) Some apsects of the behavior of the freshwater jellyfish *craspedacusta sp.* Am Nat 72:464-472

Payne F (1924) A study of the fresh-water medusa, *craspedacusta ryderi*. J Morphol 38:387-411

Pennak RW (1956) The fresh-water jellyfish *craspedacusta* in colorado with some remarks on its ecology and morphological degeneration. Trans Am Microsc Soc 75:324-331

Purcell JE (2003) Predation on zooplankton by large jellyfish *aurelia labiata, cyanea capillata,* and *aequorea aequorea,* in prince william sound, alaska. Mar Ecol Prog Ser 246:137-152

Purcell JE, Grover JJ (1990) Predation and food limitation as causes of mortality in larval herring at a spawning ground in british columbia. Mar Ecol Prog Ser 59:55-61
Raskoff KA (2002) Foraging, prey capture, and gut contents of the mesopelagic narcomedusa *solmissus* spp. (cnidaria: Hydrozoa). Mar Biol 141:1099-1107
Regula C, Colin SP, Costello JH, Kordula H (2009) Prey selection mechanism of ambush-foraging hydromedusae. Mar Ecol Prog Ser 374:135-144
Russell FS (1953) The medusae of the british isles volume 1: Anthomedusae, leptomedusae, limnomedusae, trachymedusae, and narcomedusae, Vol 1. Cambridge University Press, Cambridge
Sahin M, Mohseni K, Colin SP (2009) The numerical comparison of flow patterns and propulsive performances for the hydromedusae *sarsia tubulosa* and *aequorea victoria*. J Exp Biol 212:2656-2667
Sørnes TA, Hosia A, Båmstedt U, Aksnes DL (2008) Swimming and feeding in *periphylla periphylla* (scyphozoa, coronatae). Mar Biol 153:653-659
Spadinger R, Maier G (1999) Prey selection and diel feeding of the freshwater jellyfish, *craspedacusta sowerbyi*. Freshwat Biol 41:567-573
Suchman CL (2000) Escape behavior of *acartia hudsonica* copepods during interactions with scyphomedusae. J Plankton Res 22:2307-2323
Sullivan BK, Garcia JR, Klein-MacPhee G (1994) Prey selection by the scyphomedusan predator *aurelia aurita*. Mar Biol 121:335-341
Vogel S (1994) Life in moving fluids, Vol. Princeton University Press, Princeton, NJ

Table 1: A review of siphon experiments that measured threshold shear deformation rate required for response by several copepod species. Size refers to copepod prosome length.

Species	Size (mm)	Threshold deformation rate (s^{-1})	Source
Euchaete rimana	2.5	2.4	(Kiørboe et al. 1999)
Pleuromamma xiphias	5.5	4.6	(Kiørboe et al. 1999)
Labidocera madurae	3.3	6.3	(Kiørboe et al. 1999)
Acartia tonsa, adult	0.8	0.38	(Kiørboe et al. 1999)
Acartia tonsa, nauplii	0.2	6.3	(Kiørboe et al. 1999)
Acartia tonsa, nauplii	-	1.4	(Green et al. 2003)
Acartia hudsonica	1.01	2.2	(Burdick et al. 2007)
Oithona sp.	0.7	3.8	(Kiørboe et al. 1999)
Eurytemora affinis	1	1.9	(Kiørboe et al. 1999)
Eurytemora affinis, nauplii	-	1.0	(Green et al. 2003)
Temora longicornis	1	6.5	(Kiørboe et al. 1999)
Temora longicornis	0.74	2.7	(Burdick et al. 2007)
Temora longicornis, nauplii	-	1.5	(Green et al. 2003)
Calanus finmarchicus	0.25	0.4	(Kiørboe et al. 1999)
Tortanus discaudatus	1.22	0.34	(Burdick et al. 2007)
Centropages hamatus	1.24	1.2	(Burdick et al. 2007)

Table 2: Estimated encounter volume rates and clearance rates for Craspedacusta based on calculations from empirical data.

Encounter volume rate (±SD) [L predator^{-1} hr^{-1}]	**Prey**	**Clearance rate [L predator^{-1} hr^{-1}]**	**Source**
1.4±0.50	-	-	Aerosol filtration
7.11±2.59	-	-	Sieving
-	-	0.04	(Dodson & Cooper 1983)
-	-	0.008	(Spadinger & Maier 1999)
-	*Bosmina longirostris*	0.007	(Jankowski et al. 2005)
-	Other cladocerans	0.01	(Jankowski et al. 2005)
-	Nauplii	0.01	(Jankowski et al. 2005)
-	Copepodids	0.008	(Jankowski et al. 2005)
-	Cyclopoids (adult)	0.001	(Jankowski et al. 2005)

*Dodson and Cooper (1983) also report clearance rates up to 2.7 L predator^{-1} hour^{-1} for large nekton killed but not ingested

FIGURE LEGENDS

Figure 1: Colin et al. (2006)'s Figure 7; a diagram showing the typical flow field for rowing medusae [A] and how the flow differs around aboral tentacles [B] and oral tentacles [C], demonstrating that flow around the whole bell does not change with tentacle posture.

Figure 1: Schematic diagram of a medusa viewed from above [A] and in cross-section [B] showing parameters used in gap width calculations.

Figure 2: Contours of absolute fluid velocity magnitude for 6 states (t = time in seconds; U_{bell} = bell velocity in mm s^{-1}) representing an entire pulse cycle for a single individual, with an image of the medusa overlaid. Full pulse was 0.720 s. Values from the right side of the bell only were used in further analysis to eliminate effects from the shadow from the PIV laser on the left.

Figure 3: Contours of deformation rate (rate of strain) for 6 states (t = time in seconds; U_{bell} = bell velocity in mm s^{-1}) representing an entire pulse cycle for a single individual, with an image of the medusa overlaid. Full pulse was 0.720 s. Values from the right side of the bell only were used in further analysis, as the shadow from the PIV laser on the left generated falsely large deformation rate values. Cross-shaped, pixilated patches of concentrated high deformation rates distributed randomly throughout the strain contours represented an artifact from the computerized calculation.

Figure 4: Contours of deformation rate for State 4 for all individuals, with an image of the medusa overlaid (U_{bell}=bell velocity in mm s^{-1}). Peak deformation rates upstream of the bell occurred during this state. Values from the right side of the bell only were used in further analysis, since the shadow from the PIV laser on the left generated falsely large values. Cross-shaped, pixilated patches of concentrated high deformation rates represented an artifact from the calculation.

Figure 5: Mean values of relative velocity (u_i) between an individual medusa's long [A] and medium [B] tentacles and the surrounding fluid for 6 states representing an entire pulse cycle. Error bars indicate

standard deviation. Full pulse was 0.720 s. Bars labeled L, M, and S represent the length of the long, medium, and short tentacles, respectively. Points beyond the length of the bars represent free-stream fluid velocities. Lower velocities within the length of the short tentacles indicate the bell's boundary layer. Schematic shows posture of medium and long tentacles, and dotted lines indicate transects along which velocity profiles were measured.

Figure 6: Boundary layer thickness and gap width between tentacles along the length of the medium-sized tentacles. The 6 states in sequence represent an entire pulse cycle. Line labeled S illustrates the maximum length of the short tentacles.

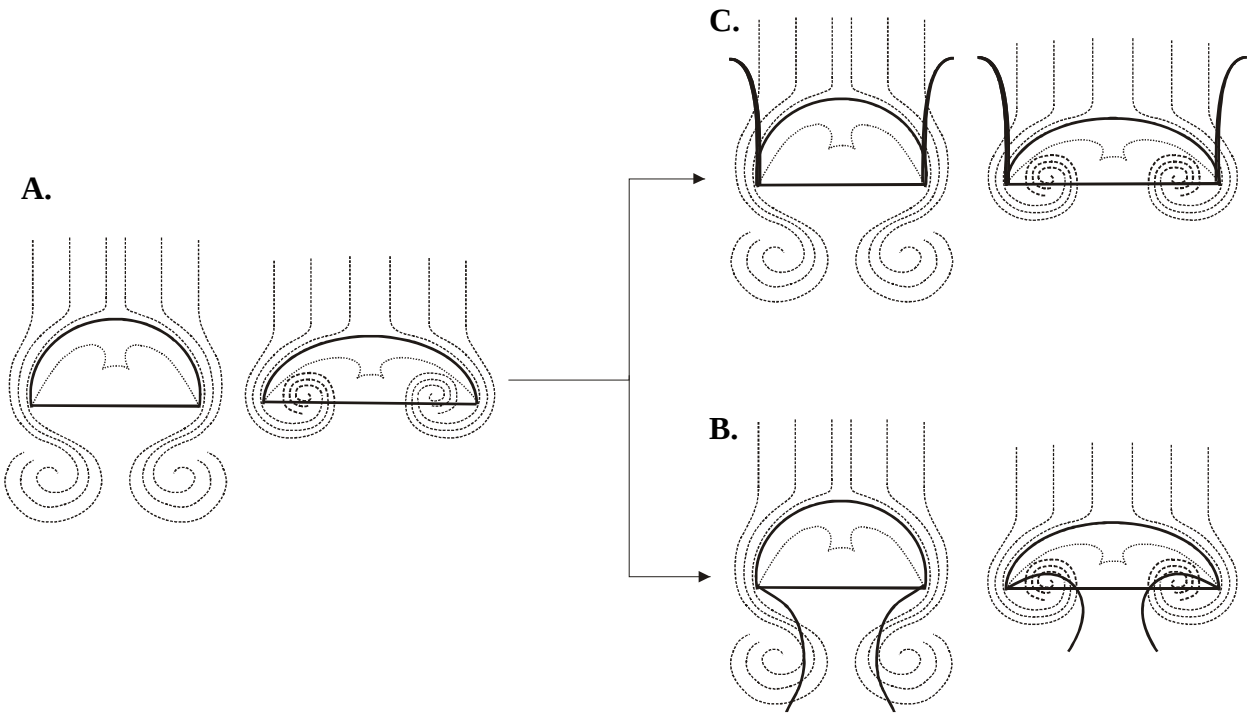

Figure 1: Colin et al. (2006)'s Figure 7; a diagram showing the typical flow field for rowing medusae [A] and how the flow differs around aboral tentacles [B] and oral tentacles [C], demonstrating that flow around the whole bell does not change with tentacle posture.

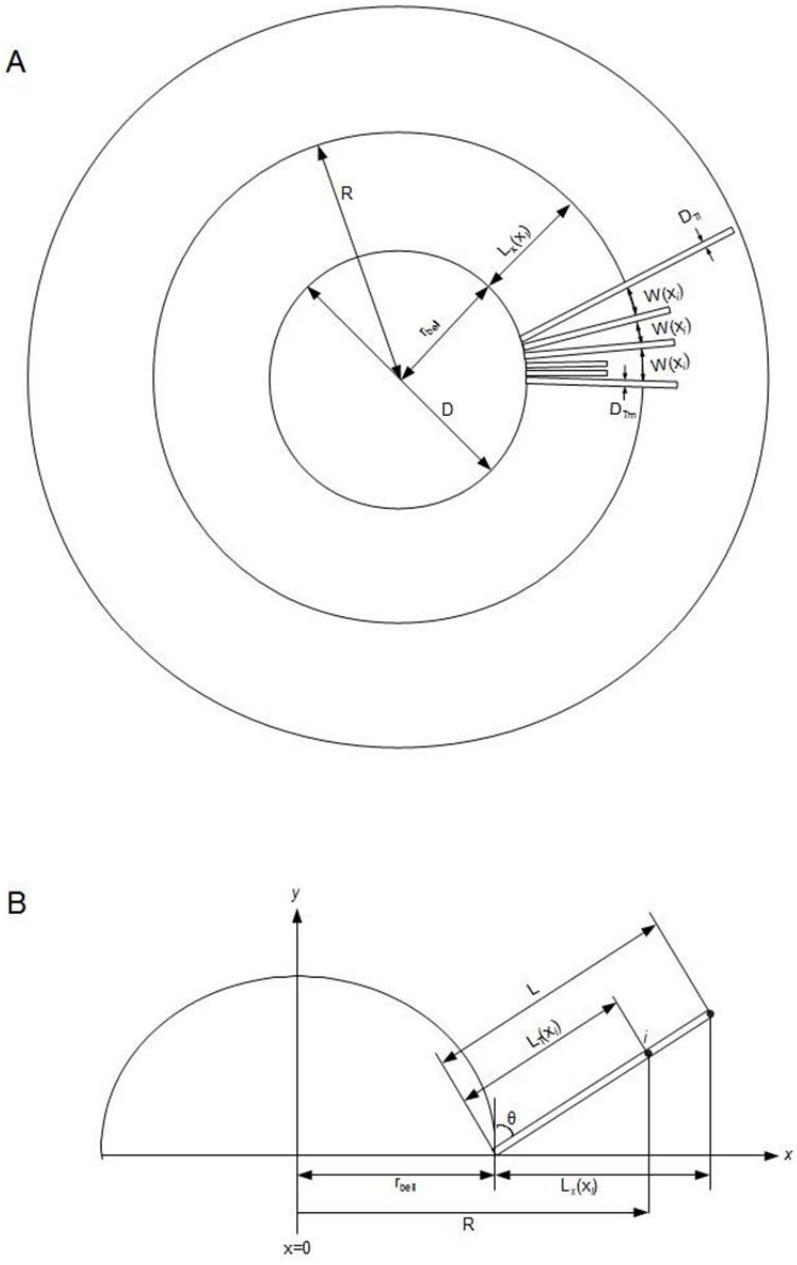

Figure 2: Schematic diagram of a medusa viewed from above [A] and in cross-section [B] showing parameters used in gap width calculations.

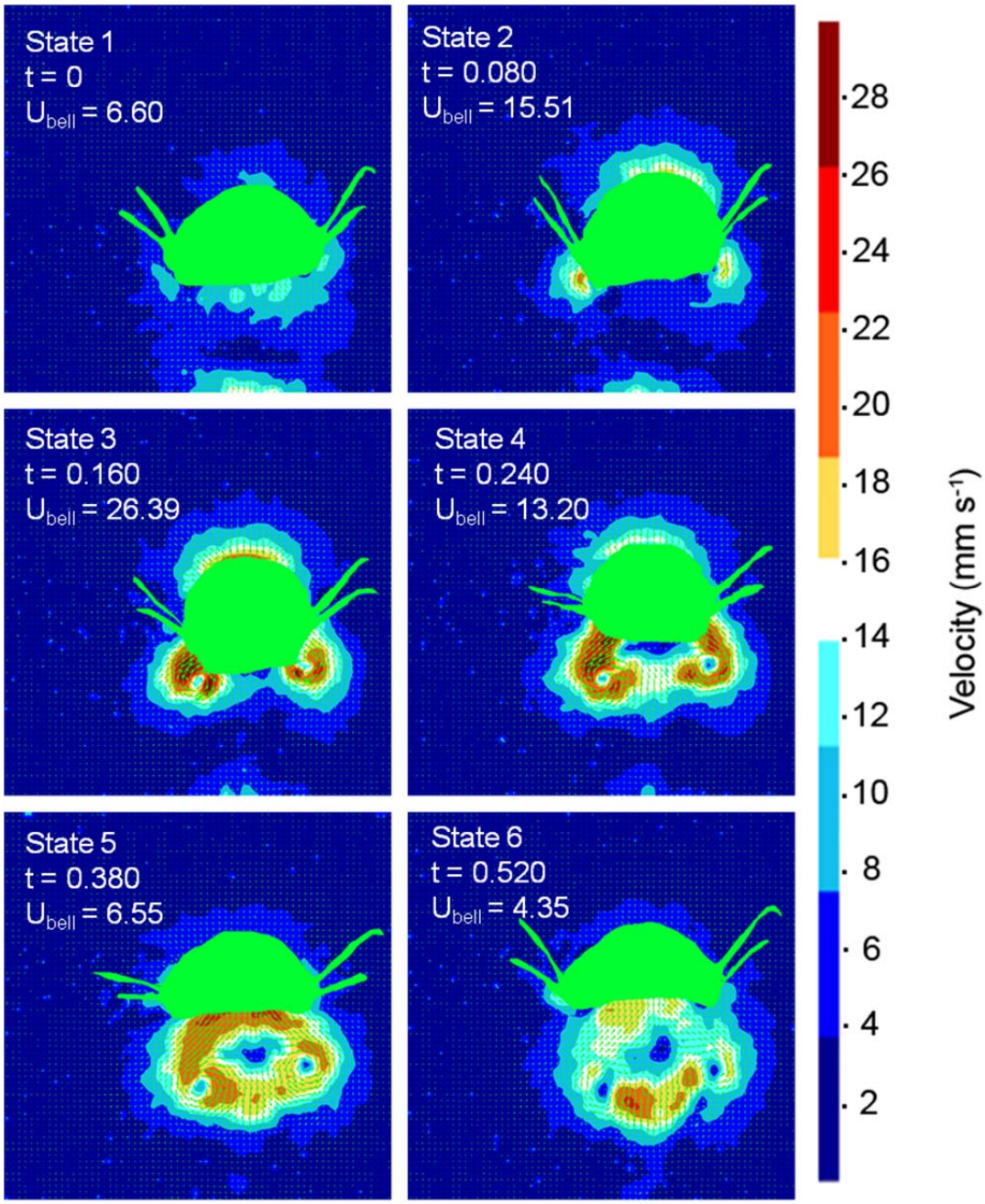

Figure 3: Contours of absolute fluid velocity magnitude for 6 states (t = time in seconds; U_{bell} = bell velocity in mm s^{-1}) representing an entire pulse cycle for a single individual, with an image of the medusa overlaid. Full pulse was 0.720 s. Values from the right side of the bell only were used in further analysis to eliminate effects from the shadow from the PIV laser on the left.

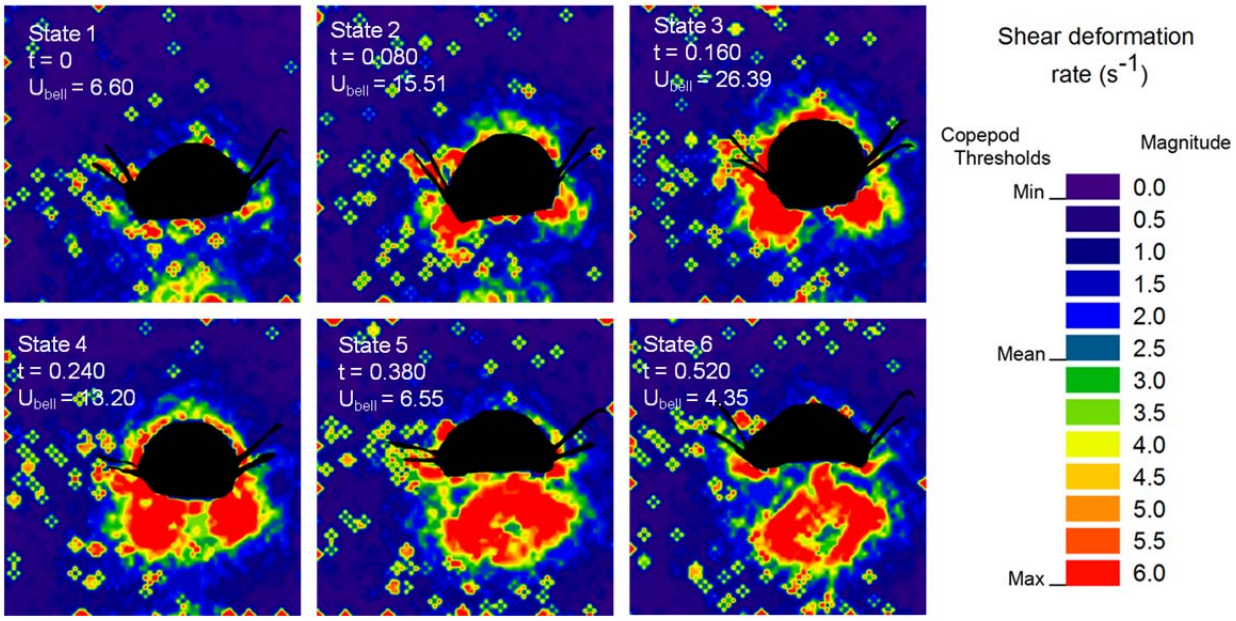

Figure 4: Contours of deformation rate (rate of strain) for 6 states (t = time in seconds; U_{bell} = bell velocity in mm s^{-1}) representing an entire pulse cycle for a single individual, with an image of the medusa overlaid. Full pulse was 0.720 s. Values from the right side of the bell only were used in further analysis, as the shadow from the PIV laser on the left generated falsely large deformation rate values. Cross-shaped, pixilated patches of concentrated high deformation rates distributed randomly throughout the strain contours represented an artifact from the computerized calculation.

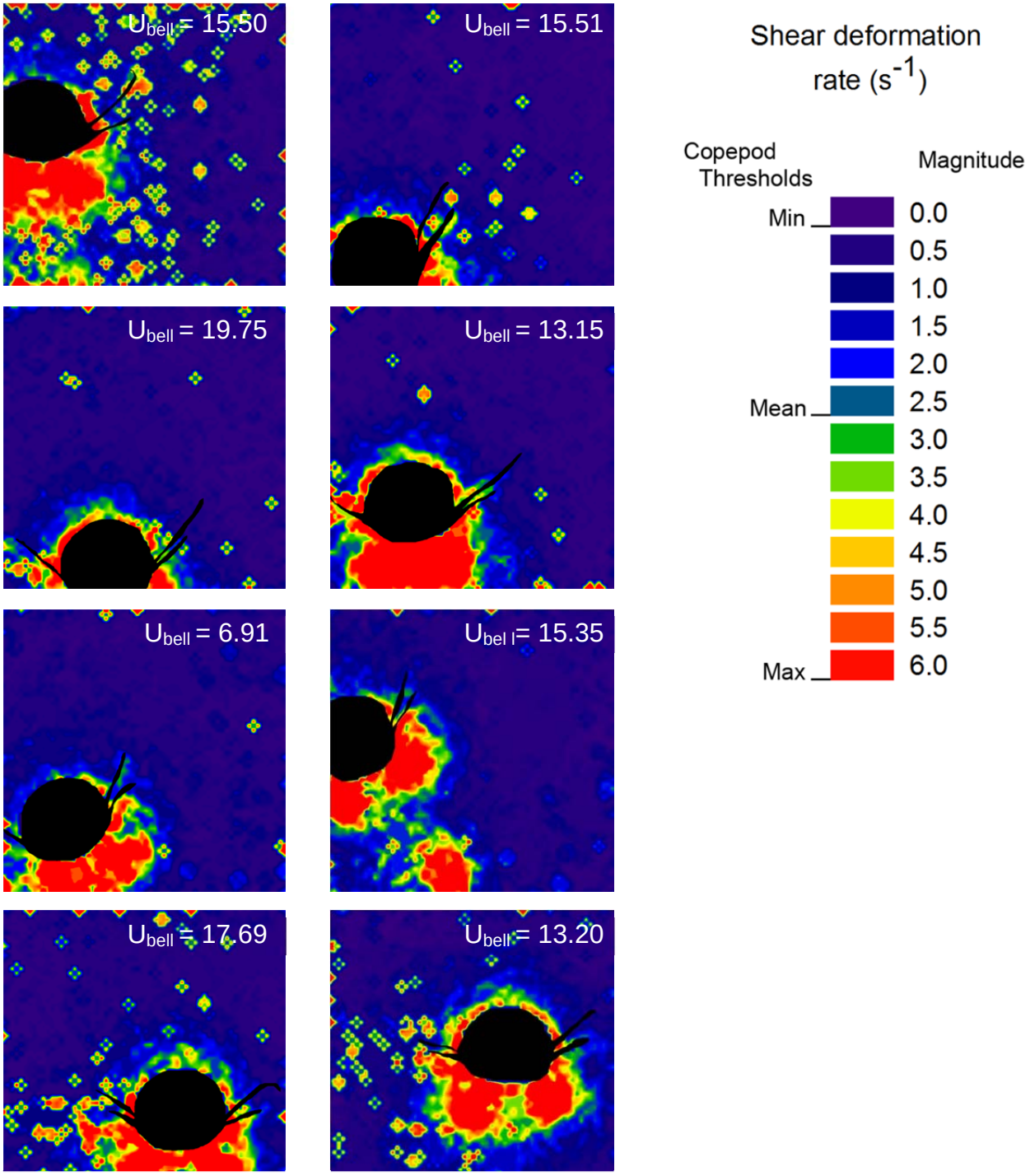

Figure 5: Contours of deformation rate for State 4 for all individuals, with an image of the medusa overlaid (U_{bell}=bell velocity in mm s^{-1}). Peak deformation rates upstream of the bell occurred during this state. Values from the right side of the bell only were used in further analysis, since the shadow from the PIV laser on the left generated falsely large values. Cross-shaped, pixilated patches of concentrated high deformation rates represented an artifact from the calculation.

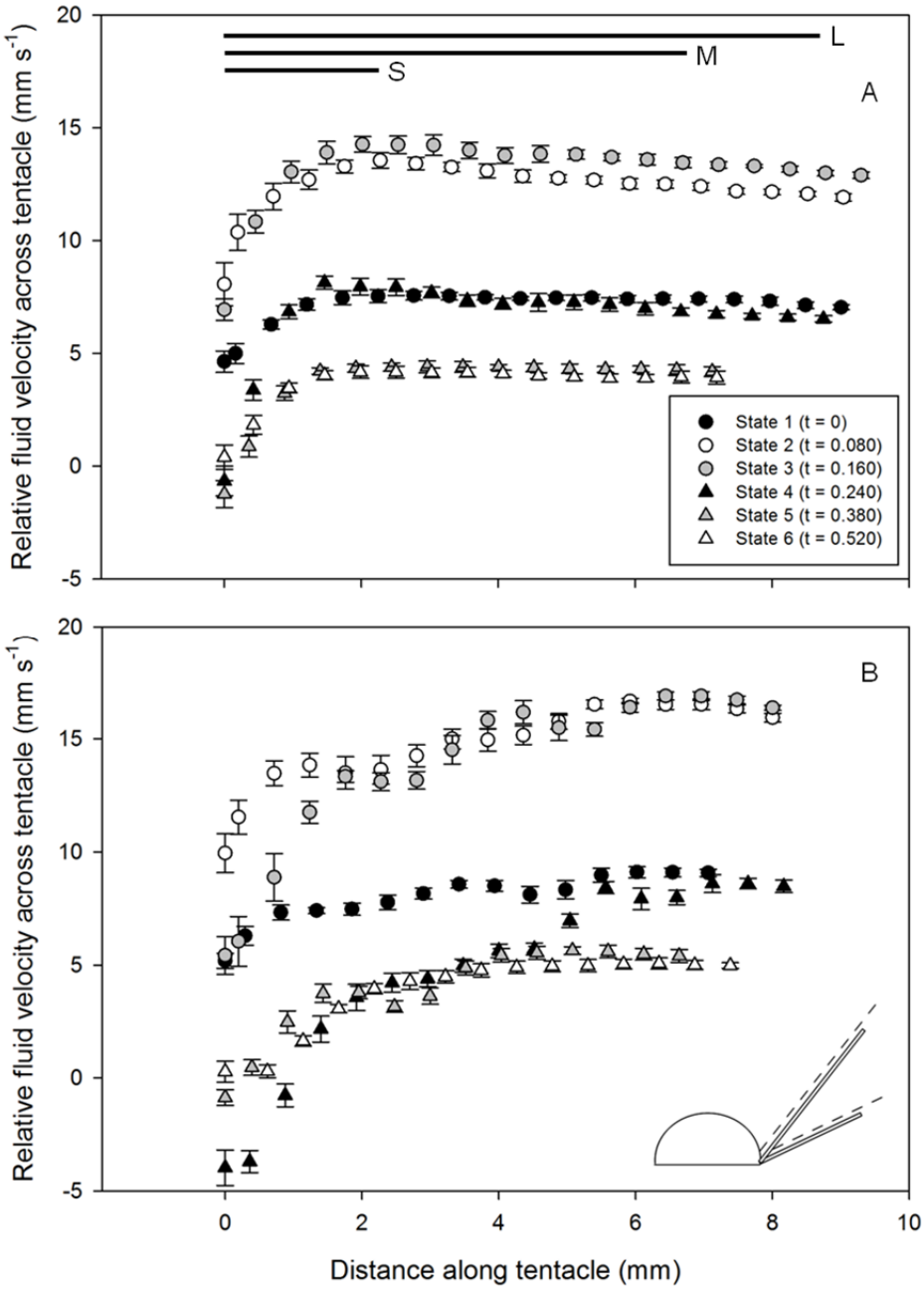

Figure 6: Mean values of relative velocity (u_i) between an individual medusa's long [A] and medium [B] tentacles and the surrounding fluid for 6 states representing an entire pulse cycle. Error bars indicate standard deviation. Full pulse was 0.720 s. Bars labeled L, M, and S represent the length of the long, medium, and short tentacles, respectively. Points beyond the length of the bars represent free-stream fluid velocities. Lower velocities within the length of the short tentacles indicate the bell's boundary layer. Schematic shows posture of medium and long tentacles, and dotted lines indicate transects along which velocity profiles were measured.

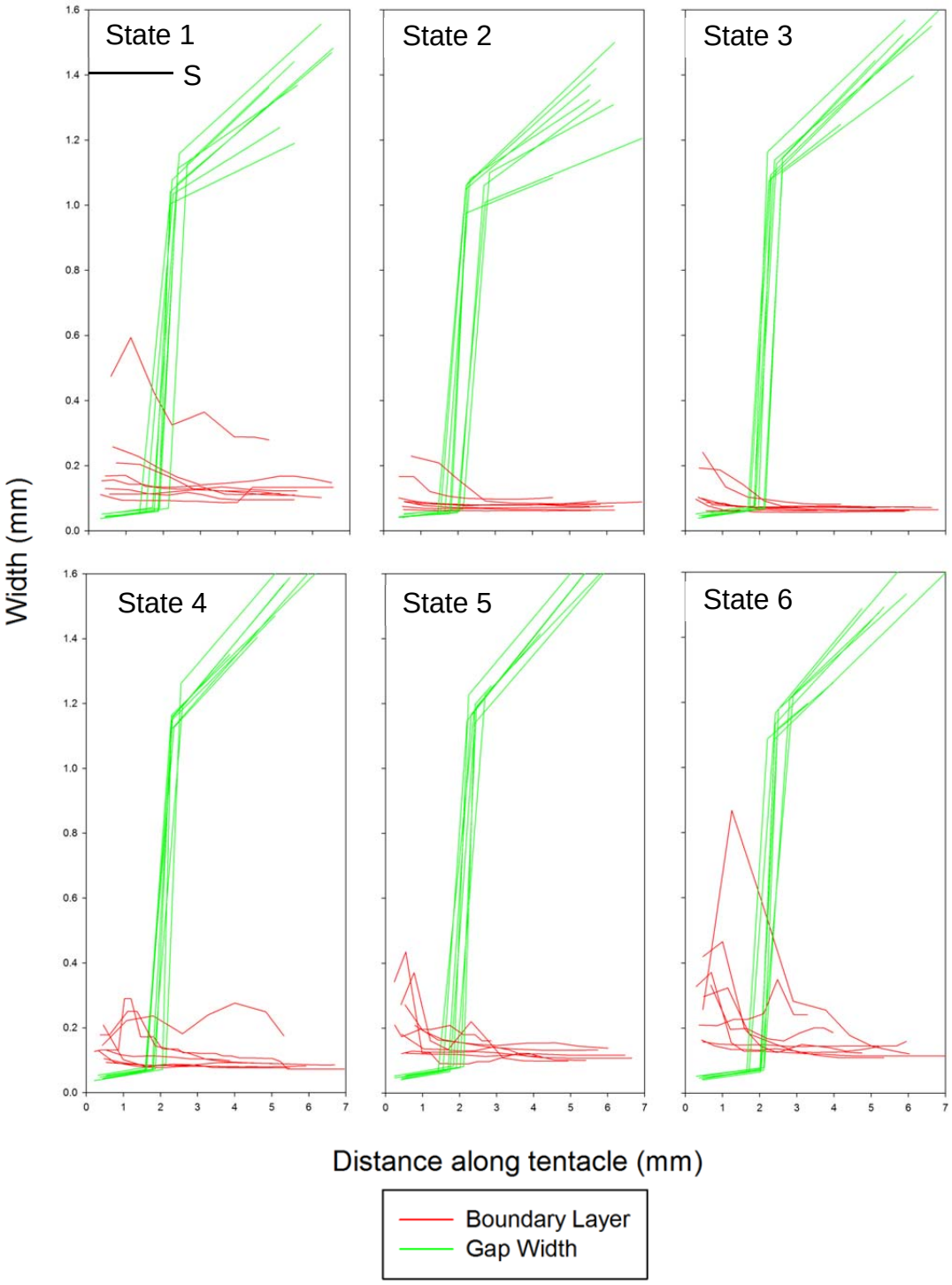

Figure 7: Boundary layer thickness and gap width between tentacles along the length of the medium-sized tentacles. The 6 states in sequence represent an entire pulse cycle. Line labeled S illustrates the maximum length of the short tentacles.